Mobility and intrinsic performance of silicon-based Nanosheet FETs at 3nm CMOS and beyond

Ali Rezaei
Device Modelling Group
James Watt School of Engineering
University of Glasgow, UK
ali.rezaei@glasgow.ac.uk

Nikolas Xeni
Device Modelling Group
James Watt School of Engineering
University of Glasgow, UK
nikolas.xeni@glasgow.ac.uk

Naveen Kumar
Device Modelling Group
James Watt School of Engineering
University of Glasgow, UK
naveen.kumar@glasgow.ac.uk

Tapas Dutta
Device Modelling Group
James Watt School of Engineering
University of Glasgow, UK
tapas.dutta@glasgow.ac.uk

Ankit Dixit
Device Modelling Group
James Watt School of Engineering
University of Glasgow, UK
ankit.dixit@glasgow.ac.uk

Ismail Topaloglu
Device Modelling Group
James Watt School of Engineering
University of Glasgow, UK
ismail.topaloglu@glasgow.ac.uk

Preslav Aleksandrov
Device Modelling Group
James Watt School of Engineering
University of Glasgow, UK
preslav.aleksandrov@glasgow.ac.uk

Vihar P. Georgiev
Device Modelling Group
James Watt School of Engineering
University of Glasgow, UK
vihar.georgiev@glasgow.ac.uk

Asen Asenov
Device Modelling Group
James Watt School of Engineering
University of Glasgow, UK
asen.asenov@glasgow.ac.uk

***Abstract*—Nanosheet Field-Effect Transistors (NSFETs) have been introduced in the 3nm CMOS technology due to their advantages over the FinFET technology. In this paper, using our in-house NanoElectronics Simulation Software (NESS), we explore the carrier mobility and the intrinsic performance of NSFETs for different channel orientations. The effective masses for different cross-sections and channel orientations are extracted from the first principal simulations. The mobility and the intrinsic performance are evaluated using the effective mass approximation non-equilibrium Green's function (NEGF) simulation engine of NESS. The proposed work provides insight into the optimized NSFET design considerations suitable for 3nm and further technology nodes.**

***Keyword-component*—Nanosheet, field-effect transistors, NSFET, NEGF, electronic band, QuantumATK, first principle, NESS**

I. Introduction

NSFETs have already been adopted in 3nm CMOS technology and show potential for 2nm CMOS and beyond. The nanometer thickness of NSFETs is more easily achievable if compared to FinFETs due to the planar orientation of the channel compared to the vertical orientation in FinFETs [1]. However, the reduction of the NSFET thickness and cross-section dimension changes the band structure and the key transport parameters compared to the bulk values that require multi-subband transport in order to accurately capture the device's performance. The crystallographic orientation of the channel material can significantly impact the electronic and transport properties of NSFETs [2], [3]. NSFETs with [100] channel orientation show excellent device performance in comparison to [110] and [111] channel orientations. This is due to the symmetry of the crystal structure, which allows for better alignment of the atoms, leading to better charge transport and current. NSFETs with [110] orientation have higher electron mobility than those with [100] orientation due to their anisotropic crystal structure. The [111] orientation is the least commonly used crystal orientation in NSFETs due to its high surface energy, which also makes it difficult

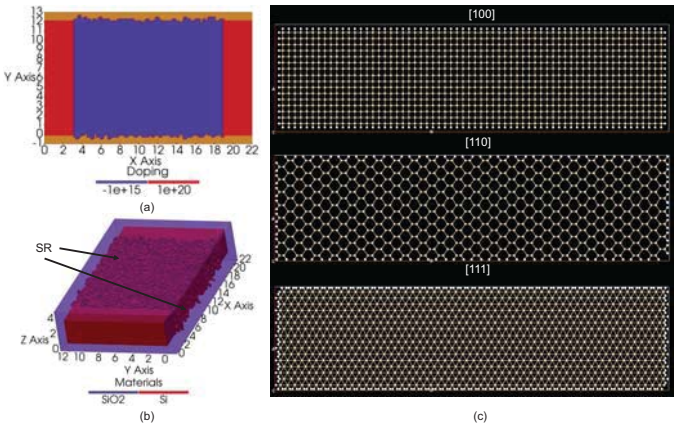

Fig. 1. (a) The SG two-dimensional representation of the doping profile of the 3nm×12nm NSFET, cross-section of the z-axis along the channel. (b) The SG three-dimensional representation of the 3nm×12nm NSFET section shows the Surface Roughness variability of the channel. (c) The crystalline cross-section from QATK for orientations [100] (top), [110] (middle), and [111] (bottom).

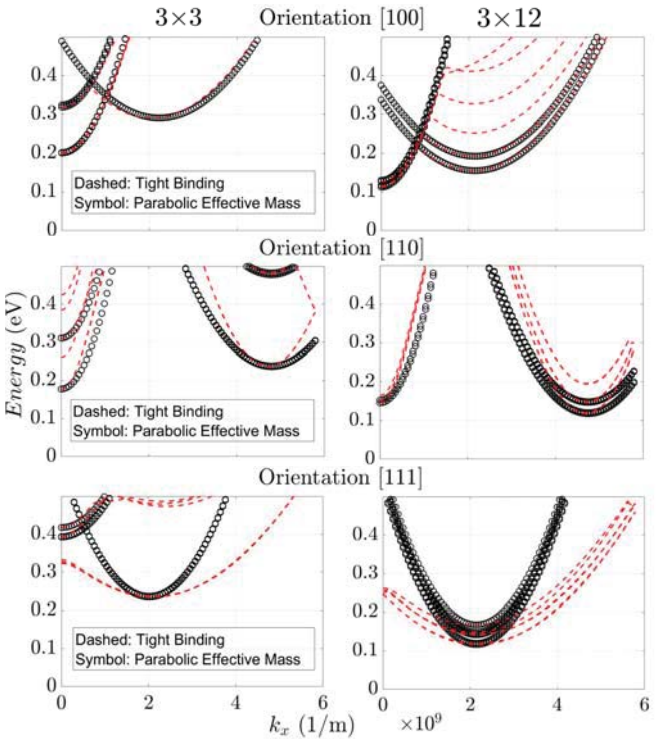

Fig. 2. Comparison of the lowest conduction band minima of the QATK TB and the Parabolic approximation from NESS EME for cross-sections (left panel) 3nm×3nm and (right panel) 3nm×12nm – orientations [100] (top), [110] (middle), and [111] (bottom). The subband minima and curvature at the minima are found to be in good agreement for all three orientations.

to grow. However, all of these NSFETs are gate-all-around architectures, and any surface defects on the channel can result in fluctuations in the leakage current and on/off ratios.

The cross-sectional dimensions of the NSFETs are another key factor that also significantly impacts their performance [4], [5]. As the cross-sectional size decreases, the transistor's dimensions approach the quantum confinement limits, which impacts the electronic properties of the channel material. A smaller cross-sectional size leads to a higher surface-to-volume ratio, which increases surface effects and, as a result, decreases carrier mobility, resulting in poor device performance [6]. Therefore, understanding the effect of different cross-section shapes and dimensions on the performance of NSFETs is crucial.

II. Methodology

The cross-sections of devices simulated in this work are illustrated in Fig. 1(a). They represent an aggressive version of the 3nm CMOS technology, with a channel cross-section of 3nm×12nm and a 1nm oxide thickness surrounding it. In this study, we consider only n-channel transistors, although NESS [7], [8] also have a p-channel NEGF engine. The NESS Structure Generator (SG) can introduce the common sources of statistical variability. Here, we have applied Surface Roughness (SR) at the channel/oxide interface as shown in Fig. 1(b), which will be used when the effects of surface roughness and confinement fluctuation scattering are investigated.

The simulation flow starts with the first principle band structure simulations using QuantumATK [9] for various cross-sections and channel orientations, as shown in Fig. 1(c). All dangling bonds are hydrogen-passivated. The Effective Mass Extractor (EME) module included in NESS is used to extract the transport and confinement effective masses by using parabolic band approximation with the correct minima extracted from the sub-band dispersion relations. In Fig. 2, we have shown that our parabolic approximation is in agreement with the minima of the conduction band for all three orientations and for both the 3nm×3nm and 3nm×12nm cross-sections. Accordingly, the extracted effective masses for each orientation for multiple cross-sections, from 3nm×3nm up to 3nm×12nm, are simulated as shown in table I.

TABLE II
The fixed parameters for the deformation potentials and energies considered for different branches in the optical scattering mechanism. The D_P for acoustic phonon is set to 14.5 eV.

Optical Phonon Type	D_P (eV/m)	Energy (eV)
g-type, TA	5×10^9	0.012
g-type, LA	8×10^9	0.0185
g-type, LO	11×10^{10}	0.063
f-type, TA	3×10^9	0.0189
f-type, LA	2×10^{10}	0.0474
f-type, TO	2×10^{10}	0.059

The quantum transport calculations are self-consistently coupled to a three-dimensional Poisson solver. For our simulations in the coupled-mode space using the effective mass approximation, we first solve the two-dimensional Schrödinger equation at each slice of the device to determine the confinement cross-section's eigenvalues and eigenfunctions. These slices are then coupled along the direction of transport, and the carrier transport is estimated using a one-dimensional NEGF solver [10] that employs the recursive Green's function algorithm [11]. Moreover, Table II represents the deformation potentials and energies for intra- and inter-valley transitions within the optical scattering mechanism.

III. Results and Discussions

Utilizing the values mentioned in Table I and II, in fig 4, we present the ballistic, total acoustic, and optical electron-phonon (PH), and PH+SR scattering I_D-V_G characteristics of two types of device cross-section, i.e., strong 3D confinement (3nm×3nm) and 2D confinement masses (3nm×12nm).

As expected, we can conclude that for all devices, the ballistic drive current (I_{ON}) is higher compared to the current including the scattering mechanisms. Also, there is a minimal difference in the leakage current (I_{OFF}) for all orientations. Consistently with the physics and the theory, both I_{ON} and I_{OFF} currents increase with the increase of the cross-section dimension, with a slight decrement in I_{ON}/I_{OFF} ratio due to

TABLE I

EXTRACTED CONFINEMENT (M_y AND M_z) AND TRANSPORT (M_x) EFFECTIVE MASSES FROM THE EME MODULE OF NESS FOR NSFETS WITH CHANNELS ORIENTED ALONG [100], [110], AND [111] DIRECTIONS ACROSS FOUR DIFFERENT CROSS-SECTIONS (SILICON WIDTH) WITH 3NM SILICON HEIGHT.

		[100]			[110]			[111]		
Width [nm]	Valley	$\mathbf{m}_y$ [$\mathbf{m}_0$]	$\mathbf{m}_z$ [$\mathbf{m}_0$]	$\mathbf{m}_x$ [$\mathbf{m}_0$]	$\mathbf{m}_y$ [$\mathbf{m}_0$]	$\mathbf{m}_z$ [$\mathbf{m}_0$]	$\mathbf{m}_x$ [$\mathbf{m}_0$]	$\mathbf{m}_y$ [$\mathbf{m}_0$]	$\mathbf{m}_z$ [$\mathbf{m}_0$]	$\mathbf{m}_x$ [$\mathbf{m}_0$]
3	Δ_x	0.278	0.278	0.945	0.496	0.259	0.568	0.763	0.22	0.455
	Δ_y	1.03	0.251	0.271	0.489	0.258	0.568	0.765	0.218	0.455
	Δ_z	0.251	0.993	0.271	0.303	0.908	0.164	0.229	0.661	0.455
6	Δ_x	0.239	0.273	0.935	0.257	0.374	0.509	0.316	0.371	0.428
	Δ_y	0.524	0.372	0.24	0.263	0.361	0.509	0.32	0.356	0.428
	Δ_z	0.544	0.36	0.24	0.955	0.28	0.159	0.417	0.28	0.428
9	Δ_x	0.478	0.281	0.954	0.587	0.375	0.526	1.116	0.383	0.426
	Δ_y	1.167	0.375	0.239	0.61	0.363	0.526	1.089	0.368	0.426
	Δ_z	1.274	0.36	0.239	2.303	0.284	0.169	1.189	0.307	0.426
12	Δ_x	0.206	0.281	0.959	0.265	0.377	0.518	0.279	0.378	0.427
	Δ_y	0.525	0.375	0.236	0.274	0.364	0.518	0.268	0.366	0.427
	Δ_z	0.592	0.362	0.236	1.049	0.281	0.171	0.295	0.303	0.427

the loss of the electrostatic gate control. In summary, our work shows that NSFET with [110] crystal orientation and 3nm×3nm cross-section offers the highest I_{ON}, and therefore performs the best in comparison to [100] and [111] devices both at low and high drain bias. Looking at the I_{ON} taken at V_G=0.7V and V_D=0.05V for the strong-confinement case, the [110] channel orientation offers drive current 1.1 (1.07) times higher than the [100] orientation and 1.29 (1.45) times higher than the [111] orientation for ballistic (PH+SR) transport; see Ref. [12] for a similar study. This is due to the variation in effective mass for the z-valley along the y-direction, which increases the possibility of recombination with asymmetry between the y and z-directions.

Further, we have investigated the impact of the effective masses on electron mobility in silicon-based NSFETs as a function of their width and channel orientation. The retrieved ballistic and PH+SR mobilities for 3nm×3nm and 3nm×12nm cross-sections at the 3nm technology node and varied channel orientations are shown in Fig 3.

We have applied the conventional transconductance method to extract the mobilities, and the findings are in line with the transfer characteristic shown in fig 4. It is evident that different scattering mechanisms, including phonon and surface roughness, lower the device's maximal mobility by more than 50 percent compared to the ballistic limit. Also, the [111] channel orientation has the lowest carrier mobility as a result of its lower valley splitting energy and larger transport masses.

IV. CONCLUSION

In summary, we have investigated the carrier mobility of NSFETs for various channel orientations and cross-sections using our in-house NanoElectronics Simulation Software (NESS). We demonstrated that our parabolic approximation agrees with the conduction band minima in all three orientations and for both the 3nm×3nm and 3nm×12nm cross-sections. Furthermore, the effective masses for different cross-sections and channel orientations are derived from the first principal simulations for electron transport studies carried out within the effective mass NEGF simulations. Both ballistic and electron-phonon (PH and PH+SR) transport mechanisms have been studied, and the I_D-V_G characteristics for the various nanowire cross-sections are reported accordingly. We have shown that NSFETs with [110] channel orientation outperform NSFETs with [100] and [111] channel orientation in the event of strong confinement. In addition, the conventional transconductance approach has been utilized for mobility calculation, and it has been demonstrated that the obtained results are consistent with the transfer characteristics.

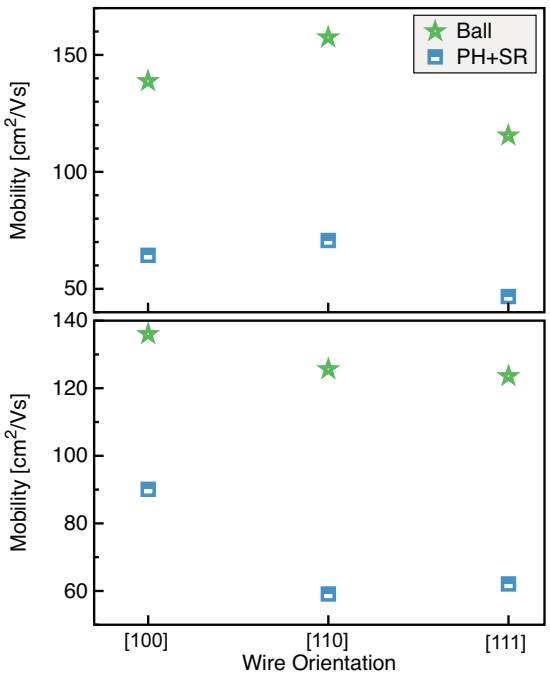

Fig. 3. Carrier mobility as a function of crystallographic orientation for (top) 3nm×3nm and (bottom) 3nm×12nm cross-section cases calculated for the 3nm (L_g=16nm) technology node. The ballistic transport and total acoustic and optical phonon (PH) combined with surface roughness (PH+SR) scattering mechanisms are considered.

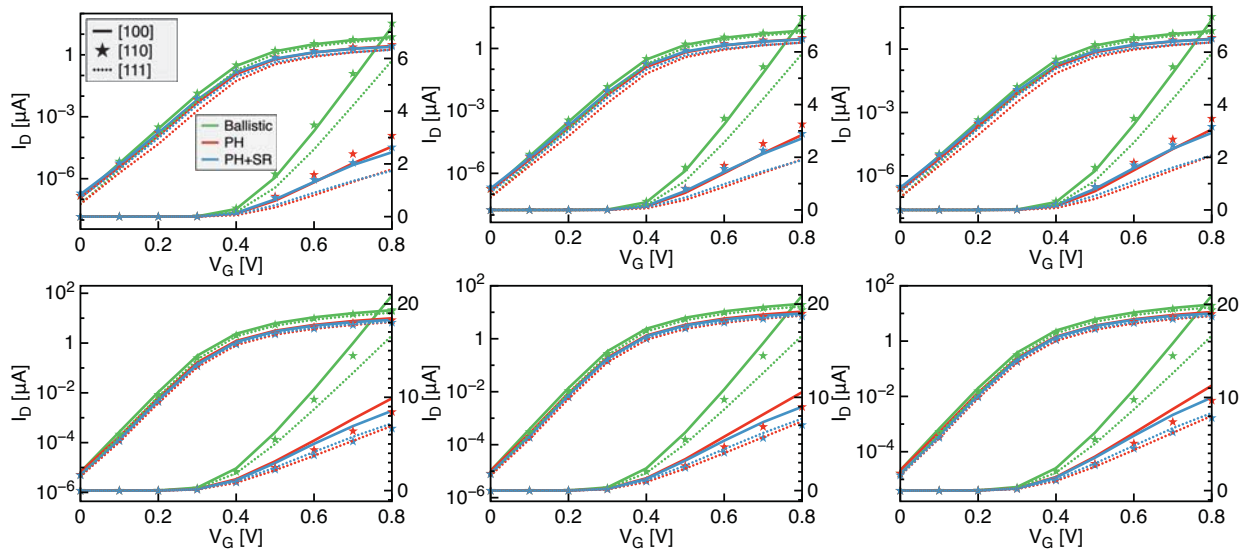

Fig. 4. (Left to right) I_D-V_G characteristics for 3nm and beyond, i.e., L_g = 16, 14, and 12nm at V_D = 0.05V for (upper panel) 3nm×3nm and (lower panel) 3nm×12nm cross-section. PH represents the total optical and acoustic electron-phonon, and PH+SR is the combined electron-phonon and SR scattering processes. The root mean square (Δ_{rms}) and correlation length (L_C) for SR scattering are set to 0.4nm and 1.3nm, respectively.

ACKNOWLEDGMENT

This research was funded by the Engineering and Physical Sciences Research Council (EPSRC), through Grant No. EP/S001131/1 and EP/P009972/1. This project has also received funding from the EPSRC Impact Acceleration Account scheme under Grant Agreement No. EP/R511705/1 (Nano-Electronic Simulation Software (NESS) – creating the first open source TCAD platform in the world and Fast Track - Development boost for the Device Modelling group opensource NESS computational framework).

REFERENCES

[1] A. Veloso, G. Eneman, T. Huynh-Bao, A. Chasin, E. Simoen, E. Vecchio, K. Devriendt, S. Brus, E. Rosseel, A. Hikavyy, R. Loo, V. Paraschiv, B. T. Chan, D. Radisic, W. Li, J. J. Versluijs, L. Teugels, F. Sebaai, P. Favia, H. Bender, E. Vancoille, J. E. Scheerder, C. Fleischmann, N. Horiguchi, and P. Matagne, "Vertical nanowire and nanosheet fets: Device features, novel schemes for improved process control and enhanced mobility, potential for faster more energy efficient circuits," in *2019 IEEE International Electron Devices Meeting (IEDM)*, 2019, pp. 11.1.1–11.1.4.

[2] Y. M. Niquet, A. Lherbier, N. H. Quang, M. V. Fernández-Serra, X. Blase, and C. Delerue, "Electronic structure of semiconductor nanowires," *Phys. Rev. B*, vol. 73, p. 165319, Apr 2006.

[3] S. Zhang, J. Z. Huang, H. Xie, A. Khaliq, D. Wang, W. Chen, K. Miao, H. Chen, and W.-Y. Yin, "Design considerations for si- and ge-stacked nanosheet pmosfets based on quantum transport simulations," *IEEE Transactions on Electron Devices*, vol. 67, no. 1, pp. 26–32, 2020.

[4] J.-S. Yoon, S. Lee, J. Lee, J. Jeong, H. Yun, and R.-H. Baek, "Reduction of process variations for sub-5-nm node fin and nanosheet fets using novel process scheme," *IEEE Transactions on Electron Devices*, vol. 67, no. 7, pp. 2732–2737, 2020.

[5] D. Jang, D. Yakimets, G. Eneman, P. Schuddinck, M. G. Bardon, P. Raghavan, A. Spessot, D. Verkest, and A. Mocuta, "Device exploration of nanosheet transistors for sub-7-nm technology node," *IEEE Transactions on Electron Devices*, vol. 64, no. 6, pp. 2707–2713, 2017.

[6] P. Ye, T. Ernst, and M. V. Khare, "The last silicon transistor: Nanosheet devices could be the final evolutionary step for moore's law," *IEEE Spectrum*, vol. 56, no. 8, pp. 30–35, 2019.

[7] C. Medina-Bailon, T. Dutta, A. Rezaei, D. Nagy, F. Adamu-Lema, V. P. Georgiev, and A. Asenov, "Simulation and modeling of novel electronic device architectures with ness (nano-electronic simulation software): A modular nano tcad simulation framework," *Micromachines*, vol. 12, no. 6, 2021.

[8] A. Rezaei, P. Maciazek, A. Sengupta, T. Dutta, C. Medina-Bailon, A. Asenov, and V. P. Georgiev, "Statistical device simulations of iii-v nanowire resonant tunneling diodes as physical unclonable functions source," *Solid-State Electronics*, vol. 194, p. 108339, 2022.

[9] K. Stokbro, D. E. Petersen, S. Smidstrup, A. Blom, M. Ipsen, and K. Kaasbjerg, "Semiempirical model for nanoscale device simulations," *Phys. Rev. B*, vol. 82, p. 075420, Aug 2010.

[10] S. Berrada, H. Carrillo-Nunez, J. Lee, C. Medina-Bailon, T. Dutta, O. Badami, F. Adamu-Lema, V. Thirunavukkarasu, V. Georgiev, and A. Asenov, "Nano-electronic simulation software (ness): a flexible nano-device simulation platform," *Journal of Computational Electronics*, vol. 19, no. 3, pp. 1031–1046, Sep 2020.

[11] A. Svizhenko, M. P. Anantram, T. R. Govindan, B. Biegel, and R. Venugopal, "Two-dimensional quantum mechanical modeling of nanotransistors," *Journal of Applied Physics*, vol. 91, no. 4, pp. 2343–2354, 02 2002.

[12] J. Wang, A. Rahman, G. Klimeck, and M. Lundstrom, "Bandstructure and orientation effects in ballistic si and ge nanowire fets," in *IEEE InternationalElectron Devices Meeting, 2005. IEDM Technical Digest.*, 2005, pp. 4 pp.–533.